hadron colliders, and therefore a large number of events can be expected even if the FCNC top decays are very rare. Furthermore, because of its large mass, the top quark is inherently connected to the electroweak symmetry breaking (EWSB) sector where new physics effects are more likely to be present. Numerous experimental searches have been carried out in the top FCNC sector. Some of these searches include $t \rightarrow \gamma c/u$ [12], $t \rightarrow gc/u$ [16], $t \rightarrow Zc/u$ [18,19] and $t \rightarrow hc/u$ [20,21] in single top production or top-pair production. The present experimental bounds on these decays are $\mathcal{B}(t \rightarrow \gamma c\ (u)) < 1.7\ (0.13) \times 10^{-3}$ [12], $\mathcal{B}(t \rightarrow gc\ (u)) < 4.1\ (0.2) \times 10^{-4}$ [16], $\mathcal{B}(t \rightarrow Zc\ (u)) < 2.4\ (1.7) \times 10^{-4}$ [18,19] and $\mathcal{B}(t \rightarrow hc\ (u)) < 2.2\ (2.4) \times 10^{-3}$ [20,21]. Similar conclusions can also be seen from the following references [7,23,24].

THE EUROPEAN
PHYSICAL JOURNAL C

CrossMark

Top quark FCNCs in extended Higgs sectors

Shankha Banerjee[a] , **Mikael Chala, Michael Spannowsky**

Physics Department, Institute of Particle Physics Phenomenology, Durham University, Durham DH1 3LE, UK

© The Author(s) 2018

Abstract The large number of top quarks produced at the LHC and possible future hadron colliders allows to study rare decays of this particle. In many well motivated models of new physics, for example in non-minimal composite-Higgs models, the existence of scalar singlets can induce new flavor-violating top decays surpassing the Higgs contribution by orders of magnitude. We study the discovery prospects of rare top decays within such models and develop new search strategies to test these interactions in top pair-produced events at the LHC. We demonstrate that scales as large as 10–50 TeV can be probed. Improvements by factors of ~ 1.5 and ~ 3 can be obtained at $\sqrt{s} = 27$ TeV and $\sqrt{s} = 100$ TeV colliders respectively.

Contents

1 Introduction

Processes mediated via flavour changing neutral currents (FCNC) are very rare within the standard model (SM) of particle physics. Any experimental evidence of such processes will thus serve as a clear signal for new physics. These possible rare processes have garnered strong interest in both the theoretical and experimental communities and have triggered numerous studies in search for FCNCs, particularly in the top production [1–7] and decay channels [8–22]. Looking for such rare processes in the top sector is very lucrative because top quarks are copiously produced at high-energy hadron colliders, and therefore a large number of events can be expected even if the FCNC top decays are very rare. Furthermore, because of its large mass, the top quark is inherently connected to the electroweak symmetry breaking (EWSB) sector where new physics effects are more likely to be present. Numerous experimental searches have been carried out in the top FCNC sector. Some of these searches include $t \rightarrow \gamma c/u$ [12], $t \rightarrow gc/u$ [16], $t \rightarrow Zc/u$ [18,19] and $t \rightarrow hc/u$ [20,21] in single top production or top-pair production. The present experimental bounds on these decays are $\mathcal{B}(t \rightarrow \gamma c\ (u)) < 1.7\ (0.13) \times 10^{-3}$ [12], $\mathcal{B}(t \rightarrow gc\ (u)) < 4.1\ (0.2) \times 10^{-4}$ [16], $\mathcal{B}(t \rightarrow Zc\ (u)) < 2.4\ (1.7) \times 10^{-4}$ [18,19] and $\mathcal{B}(t \rightarrow hc\ (u)) < 2.2\ (2.4) \times 10^{-3}$ [20,21]. Similar conclusions can also be seen from the following references [7,23,24].

A priori, however, there might be other particles lurking around the Electroweak (EW) scale, into which the top quark can possibly decay. Out of the different possibilities, scalar singlets, S, constitute a prime example at the level of dimension-four interactions. When the singlet mixes with the SM-like Higgs boson, its production is strongly constrained owing to the increasingly precise Higgs signal strength measurements (central values reaching unity along with decreasing uncertainties) in various channels [25,26] and also from measurements of the W-boson mass [27–31]. For a relatively small mixing parameter of $\sin\theta$ varying between 0.2 and 0.35 [32,33], one can however, have a wide range of allowed singlet mass.

Such scalar particles are predicted by some of the best motivated models of new physics, including supersymmetric extensions (e.g., the NMSSM [34]) and Composite Higgs Models (CHM) [35–38]. Moreover, we will see that these scalars can induce FCNCs significantly larger than those mediated by the SM-like Higgs boson [39]. The reason for the above is three-fold; (i) The top FCNCs mediated by a new scalar singlet are generally suppressed by one less power of the heavy physics scale, (ii) in principle, the scalar singlet can have a larger decay width into cleaner final states, such

a e-mail: shankha.banerjee@durham.ac.uk

Springer

as $\ell^+\ell^-$, $b\bar{b}$ or $\gamma\gamma$ and (iii) in broad classes of models (*for example* in CHMs), Higgs mediated FCNCs are forbidden in first approximation [8]. Altogether, top FCNCs mediated by new scalars might be well within the reach of the LHC.

Presently, there are no direct limits on $t \to qS$. However, one can have strong constraints from $D^0 - \bar{D}^0$ oscillations [24,40,41] which always come about as a product of two S Yukawas, Y_{ct} and Y_{ut} (and also Y_{uc}). In order to circumvent these constraints, one can always fall back upon scenarios where Y_{ut} is negligibly small. We will argue in Sect. 3, that the ut FCNCs can be vanishingly small compared to their ct counterpart in explicit models.

In this work, we scrutinise the reach of the LHC for top FCNCs in top-pair produced events. We consider the standard leptonic decay of one of the tops, while the other is assumed to decay into Sc, with either $S \to b\bar{b}$ or $S \to \gamma\gamma$ (leptonic decays will be analysed in a later work). In principle, the current experimental searches for $t \to hc$ might be also sensitive to these signals. However, these searches are only optimised for a 125 GeV scalar resonance and not for the whole range of masses, in which S can potentially lie. Moreover, the latest experimental strategies (see e.g. Ref. [42]) rely on trained BDTs which make them hard to recast for arbitrary scalar masses. In light of these issues, we develop new dedicated analyses tailored for each mass point.

The structure of the paper is as follows. In Sect. 2 we outline a model-independent introduction to the signals of interest. We follow this up in Sect. 3, where we discuss concrete realisations, involving both strongly and weakly coupled models of new physics. This allows us to establish well-motivated benchmark points (BP). We go on to discuss the analysis for the $b\bar{b}$ channel in Sect. 4 and in Sect. 5, we present the corresponding analysis for the $S \to \gamma\gamma$ mode for the 14 TeV LHC machine. We finally conclude in Sect. 6, where we also provide an outlook for the high energy colliders by commenting on naive estimations of the reach of hadron colliders at $\sqrt{s} = 27$ TeV and $\sqrt{s} = 100$ TeV.

2 Effective Lagrangian

Let us consider a scenario where the SM Higgs sector is extended by a gauge singlet, S, having a mass m_S in the EW regime. For low energies, we write the relevant Yukawa Lagrangian as follows[1]

$$\mathcal{L} = -\overline{\mathbf{q_L}} \left(\mathbf{Y} + \mathbf{Y}' \frac{|H|^2}{f^2} + \tilde{\mathbf{Y}} \frac{S}{f} \right) \tilde{H} \mathbf{u_R} + \text{h.c.}, \quad (2.1)$$

where $H = [\phi^+, (h + \phi^0)/\sqrt{2}]^t$, is the SM-like Higgs doublet, $\mathbf{q_L}(\mathbf{u_R})$ denotes the left-handed (right-handed) quarks, $\mathbf{Y}, \mathbf{Y}'$, and $\tilde{\mathbf{Y}}$ are arbitrary flavour matrices, $v \sim 246$ GeV, is the Higgs vacuum expectation value (*vev*) and $f \gtrsim \mathcal{O}(\text{TeV})$ is the new physics scale. In general, the flavour matrices are not aligned, and thus the FCNCs can arise in the EW phase. Among various new physics effects, these induce top flavour-violating decays, *viz.*, $t \to hc$ or $t \to Sc$. In general, the latter dominates over the former, because (i) $t \to hc$ is further suppressed by an additional factor of $1/f$ and (ii) in several UV-complete models, $\mathbf{Y}$ and $\mathbf{Y}'$ are approximately aligned. Finally, after the EWSB, one obtains

$$\mathcal{L} = -\frac{v}{\sqrt{2}} \left[\overline{\mathbf{q_L}} \mathbf{Y} \left(1 + \frac{h}{v} \right) \mathbf{u_R} + \frac{S}{f} \overline{\mathbf{q_L}} \tilde{\mathbf{Y}} \mathbf{u_R} + \mathcal{O} \left(\frac{1}{f^2} \right) \right]$$
$$\supset \tilde{g} \frac{m_t}{f} \overline{t_L} S c_R + \text{h.c.}, \quad (2.2)$$

where $m_t \sim 173$ GeV is the top mass and g is an $\mathcal{O}(1)$ coupling. Such interactions can be tested to a high accuracy through rare top decays. Upon using Eq. 2.2, one obtains the partial width of $t \to Sc$ as follows

$$\Gamma(t \to Sc) = \frac{\tilde{g}^2}{32\pi} \frac{v^2}{f^2} m_t \left(1 - \frac{m_S^2}{m_t^2} \right)^2, \quad (2.3)$$

and thus for a benchmark point with $\tilde{g} \sim 1$ and $f \sim 1$ TeV, one obtains $\mathcal{B}(t \to Sc) \sim \Gamma(t \to Sc)/\Gamma_t^{\text{SM}} \sim 0.03$ with $\Gamma_t^{\text{SM}} \sim 1.4$ GeV [43]. A full exploration of this decay in singly or pair-produced top quarks at colliders, depends also on how S decays to SM particles. Motivated by CHMs (as discussed below), we consider a scenario where S couples to the SM fermions, ψ, via $\frac{c_\psi m_\psi}{f} S \bar{\psi} \psi$ and to the photons via $\frac{c_\gamma \alpha}{4\pi f} S F_{\mu\nu} \tilde{F}^{\mu\nu}$, where c_ψ and c_γ are arbitrary $\mathcal{O}(1)$ couplings and α is the fine-structure constant. Thus, in the regime, $m_S \gg m_\psi$, one obtains at leading order

$$\Gamma(S \to \psi\psi) = \frac{N_c}{8\pi} \frac{c_\psi^2 m_\psi^2}{f^2} m_S \quad \text{and} \quad \Gamma(S \to \gamma\gamma) = \frac{c_\gamma^2 \alpha^2}{64\pi^3 f^2} m_S^3. \quad (2.4)$$

Thus, one finds the relation $\mathcal{B}(S \to \gamma\gamma)/\mathcal{B}(S \to \overline{\psi}\psi) \sim \frac{\alpha^2}{\pi^2}(m_S/m_\psi)^2$. The suppression factor driven by the small electromagnetic coupling can thus be partially compensated upon scaling with the free parameter m_S. $\mathcal{B}(S \to \gamma\gamma)$ can

---

[1] We note that in the absence of effective operators, the interaction of S with the fermions, is negligible. Indeed, such interactions only arise at one loop (and only if S is not a pseudo-scalar; otherwise there

Footnote1 continued
is an accidental symmetry $S \to -S$, provided CP is conserved). Moreover, these are proportional to the *vev* of S, which triggers the mixing with the Higgs boson and are therefore severely constrained by current Higgs measurements [26,30,31]. In addition, the FCNC currents will be further suppressed by the GIM mechanism. Thus, we would expect $\mathcal{B}(t \to Sc)$ to be several orders of magnitude smaller than $\mathcal{B}(t \to hc)$, which in the SM is predicted to be smaller than 10^{-13} [9].

be significantly larger than the $\mathcal{B}(h \rightarrow \gamma\gamma) \sim 2 \times 10^{-3}$, with the precise value being model dependent.

3 Explicit models

The Lagrangian in Eq. 2.1 appears naturally in several UV-complete models, for example in CHMs. In these classes of models, H and S are pseudo Nambu-Goldstone Bosons (pNGBs) arising in a new global symmetry breaking $\mathcal{G}/\mathcal{H}$ at a scale $\sim f$. A prime example is the CHM based on the coset $SO(6)/SO(5)$ [44], which is the smallest one that admits four-dimensional UV completion [45]. The generators of this coset can be chosen as

$$T_{ij}^{mn} = -\frac{\mathrm{i}}{\sqrt{2}}\left(\delta_i^m \delta_j^n - \delta_i^n \delta_j^m\right), \quad m < n \in [1, 5], \tag{3.1}$$

$$X_{ij}^{m6} = -\frac{\mathrm{i}}{\sqrt{2}}\left(\delta_i^m \delta_j^6 - \delta_i^6 \delta_j^m\right), \quad m \in [1, 5]. \tag{3.2}$$

Among these, $X^{16} - X^{46}$ expand the coset space of the Higgs doublet, while the broken generator associated to S is provided by X^{56}. The SM fermions do not couple directly to the (fully composite) Higgs. Instead, the latter couples to composite fermionic resonances, which in turn mix with the SM fermions, thus explicitly breaking the global symmetry. The Yukawa Lagrangian depends therefore on the quantum numbers of the aforementioned fermionic resonances. For concreteness, we will assume that these fields transform in the fundamental representation $\mathbf{6}$ of $SO(6)$. The latter can be decomposed as $\mathbf{6} = \mathbf{1} + \mathbf{1} + \mathbf{4}$ under the custodial symmetry group $SO(4)$. Let us assume that u_R^i is embedded in both singlets, whereas the one for q_L^i is fixed. These are listed as

$$U_{R_1}^i = \left(0, 0, 0, 0, \mathrm{i}u_R^i, 0\right), \quad U_{R_2}^i = \left(0, 0, 0, 0, 0, u_R^i\right) \tag{3.3}$$

and $\quad Q_L^i = \frac{1}{\sqrt{2}}\left(\mathrm{i}b_L^i, b_L^i, \mathrm{i}t_L^i, -t_L^i, 0, 0\right). \tag{3.4}$

Using the corresponding Goldstone matrix

$$\mathrm{U} = \begin{bmatrix} 1_{3\times3} & & & \\ & 1 - h^2/(f^2+\Pi) & -hs/(f^2+\Pi) & h/f \\ & -hs/(f^2+\Pi) & 1 - S^2/(f^2+\Pi) & S/f \\ & -h/f & -S/f & \Pi/f^2 \end{bmatrix},$$

$$\Pi = f^2\left(1 - \frac{h^2}{f^2} - \frac{S^2}{f^2}\right)^{1/2}, \tag{3.5}$$

one obtains the Yukawa Lagrangian

$$L = -f y_{ij}^{(1)} \overline{(\mathrm{U}^T Q_L^i)}_6 \left(\mathrm{U}^T U_{R_1}^j\right)_6 - f y_{ij}^{(2)} \overline{(\mathrm{U}^T Q_L^i)}_6 \left(\mathrm{U}^T U_{R_2}^j\right)_6 + \text{h.c.}$$

$$= -\frac{1}{\sqrt{2}} \overline{q_L^i} h t_R^j \left[y_{ij}^{(2)}\left(1 - \frac{h^2}{f^2} - \frac{S^2}{f^2}\right)^{1/2} + \mathrm{i} y_{ij}^{(1)} \frac{S}{f} \right] + \text{h.c.}, \tag{3.6}$$

which, to leading order, reads

$$L = -\frac{1}{\sqrt{2}} \overline{q_L^i} h t_R^j \left[y_{ij}^{(2)} - y_{ij}^{(2)} \frac{h^2}{2f^2} + \mathrm{i} y_{ij}^{(1)} \frac{S}{f} + \cdots \right] + \text{h.c.} \tag{3.7}$$

Hence, we obtain $\mathbf{Y}_{ij} = -\mathbf{Y}' = y_{ij}^{(2)}$ and $\tilde{\mathbf{Y}}_{ij} = \mathrm{i} y_{ij}^{(1)}$. Thus, to leading order, scalar mediated FCNCs are only driven by S, provided that $y_{ij}^{(1)}$ and $y_{ij}^{(2)}$ are not aligned. Even in that case, the FCNCs would still arise in the presence of higher-dimensional operators, and then undergo suppression by a factor of $1/g_*^2$ (with g_* being a strong coupling) just as in the minimal CHM [8,38]. Similar results hold for other representations, with the exception of those that respect a $S \rightarrow -S$ parity and those for which the shift symmetry of S remains unbroken, examples being q_L^i in the $\mathbf{6}$, t_R^i in the $\mathbf{15}$ [46].

We note that although $\tilde{\mathbf{Y}}_{ij}$ is in principle arbitrary, one can easily expect sizeable top-charm couplings and still have small top-up FCNCs. Indeed, despite being not directly measurable, in common viable *ansätze*, $\mathbf{Y}$ is hierarchical and nearly block-diagonal, with the maximal mixing occurring in the top-charm sector [47,48]. It can therefore be diagonalised as $\mathbf{Y} \rightarrow \mathbf{L}^\dagger \mathbf{Y} \mathbf{R}$, with $\mathbf{L}$ and $\mathbf{R}$ being block-diagonal as well. Moreover, in CHMs the aforementioned hierarchy reflects the fact that heavier fermions couple stronger to the composite sector, so not only to H but also to S. One can then easily expect a similar block-diagonal structure for $\tilde{\mathbf{Y}}$. As a consequence, $\mathbf{L}\tilde{\mathbf{Y}}\mathbf{R}$ is also block-diagonal with only the top-charm mixing. Hence, we concentrate on the $t \rightarrow Sc$ decay channel. However, because we will not use any explicit c-tagging in our analyses, our results can easily be translated for the $t \rightarrow Su$ mode.

We define three Benchmark Points (BP), each including $m_S = 20, 50, 80, 100, 120$ and 150 GeV, as follows

BP 1 : $\tilde{g} = 1.0$, $f = 2$ TeV $\implies \mathcal{B}(t \rightarrow Sc) \sim 10^{-3} - 10^{-2}$;

BP 2 : $\tilde{g} = 1.0$, $f = 10$ TeV $\implies \mathcal{B}(t \rightarrow Sc) \sim 10^{-4} - 10^{-3}$;

BP 3 : $\tilde{g} = 0.1$, $f = 2$ TeV $\implies \mathcal{B}(t \rightarrow Sc) \sim 10^{-5} - 10^{-4}$;

$$\tag{3.8}$$

We note that, although being *a priori* relatively light, values of $m_S < m_h/2 \sim 62.5$ GeV are not necessarily excluded by the LHC constraints on the Higgs width [49]. Actually, the latter translates into an upper bound $\Gamma(h \rightarrow SS) \lesssim 10$ MeV. Given that for a quartic coupling $\lambda_{HS} S^2 |H|^2$ one obtains $\Gamma(h \rightarrow SS) \sim \lambda_{HS}^2/(32\pi) \times v^2/m_h$, we can evade the aforementioned bound provided $\lambda_{HS} < 0.05$. Similarly, derivative interactions $\sim hS\partial h\partial S/f^2$, unavoidable

Table 1 Single field extensions of the SM supplemented with S that induce the FCNC of interest at low energy at tree level. The numbers in parenthesis and the subscript denote the $SU(3)_c$ and $SU(2)_L$ representations and the hypercharge, respectively. From the top left and clockwise, the different diagram legs represent q_L^i, t_R^j, H and S, respectively

Field	Relevant Lagrangian	Diagram	$\tilde{\mathbf{Y}}_{ij}/f^2$
$Q = (1,2)_{1/6}$	$L_Q = -m_Q \overline{Q}Q + (\alpha_i^Q \overline{Q} S q_L^i$ $+\tilde{\alpha}_j^Q \overline{Q} \tilde{H} u_R^j + \text{h.c.})$		$\dfrac{\alpha_i^Q \tilde{\alpha}_j^Q}{m_Q}$
$U = (1,1)_{2/3}$	$L_U = -m_U \overline{U}U + (\alpha_i^U \overline{U} H q_L^i$ $+\tilde{\alpha}_j^U \overline{U} S u_R^j + \text{h.c.})$		$\dfrac{\alpha_i^U \tilde{\alpha}_j^U}{m_U}$
$\Phi = (1,2)_{1/2}$	$L_\Phi = -\frac{1}{2}m_\Phi^2 \Phi^2 + (\alpha_{ij}^\Phi \overline{q_L^i} \tilde{\Phi} u_R^j$ $+\kappa S\Phi^\dagger H + \text{h.c.})$		$\dfrac{\alpha_{ij}^\Phi \kappa}{m_\Phi^2}$

in CHMs, contribute to the Higgs width with an effective $\lambda_{HS} \sim 4m_h^2/f^2 \lesssim 0.05$ for a scale, $f \gtrsim 1.2$ TeV.

If we consider only weakly-coupled extensions of the SM+S, the Lagrangian in Eq. 2.1 can also be induced *at tree level* by the fields listed in Table 1. In particular, this means that the NMSSM [34], which extends the SM scalar sector with an additional $SU(2)_L$ doublet with $Y = 1/2$ (required by SUSY itself) as well as with a singlet (in order to avoid the μ-problem [50]), fits naturally into the targets of our analysis.

4 LHC prospects for $t \to Sc$, $S \to b\bar{b}$

In this section, we focus on the scenario where the scalar singlet decays to a pair of b-quarks, yielding a final state comprised of at least four jets, three of them required to be b-tagged and exactly one isolated lepton. As described above, we quantify our results in terms of six benchmark masses, viz., $m_S = 20, 50, 80, 100, 120$ and 150 GeV. Our ultimate goal in this section is to derive an upper bound on $\mathcal{B}(t \to Sc, S \to b\bar{b})$ at 95 % Confidence Level (CL).

We have fixed the b-tagging efficiency to 70%. The c $(\ell) \to b$ mistag rate has been taken as 10% (1%). The most dominant real background ensues from semi-leptonic $t\bar{t}b\bar{b}$ production. Besides, the fully leptonic channel from the aforementioned production mode also contributes. The major fake backgrounds that we consider are the semi-leptonic (and leptonic) $t\bar{t}$ merged up to one extra matrix element parton, the $Wb\bar{b}$ process merged up to two extra matrix element partons and $Zb\bar{b}$ also merged up to two extra partons with the Z-boson decaying leptonically. For the analysis framework, we use MG5_aMC@NLO v2.6.0 [51] for generating the signal and background samples. We employ the MLM

merging scheme [52] embedded in this framework, with appropriate parameter choices. We use very loose parton level cuts, viz., $p_T(j) > 15$ GeV, $p_T(b) > 15$ GeV and $p_T(\ell) > 10$ GeV, as well as $|\eta(j)| < 4$, $|\eta(b)| < 4$ and $|\eta(\ell)| < 3$. Moreover, we require the ΔR separations to be zero for each pair at the generation level. The cross sections of $t\bar{t}$, $Wb\bar{b}$, $Zb\bar{b}$ and $t\bar{t}b\bar{b}$ are multiplied by K-factors of 1.6, 2.3, 1.25 and 1.13, respectively. While the first one can be found in Ref. [53], the other three have been estimated by computing in MG5_aMC@NLO at NLO in QCD. We use the NNPDF 2.3 [54] at leading order. The analyses in this section and in the next are carried out for the 14 TeV LHC.

Furthermore, we shower the samples with Pythia 8 [55].[2] Finally, at the analysis level, we construct the jets employing the anti-k_T [56] algorithm with a jet parameter $R = 0.4$ in the FastJet [57] framework. All the jets are required to have $p_T > 30$ GeV and to lie within a pseudorapidity range of $|\eta| < 2.5$. Leptons must have a $p_T > 10$ GeV and $|\eta| < 2.5$. For the isolation, we require that the total hadronic activity around the lepton within a cone of $\Delta R = 0.2$ is less than 10 % of its transverse momentum. All the aforementioned selected objects are also required to be separated by $\Delta R > 0.4$.

After selecting these events, we look for the closest pair (in terms of ΔR separation) of b-tagged jets and reconstruct the top-quark mass $m_t^{\Delta R}$ with the additional hardest jet which is not b-tagged. We require this variable to be within a window of 50 GeV from m_t. With the remaining b-tagged jet, we construct the transverse mass variable m_T and require it to be less than 200 GeV. We show the distributions of $m_t^{\Delta R}$, m_T and the reconstructed scalar mass, $m_S^{\Delta R}$, after the basic cuts (which include the aforementioned p_T cuts as well as a requirement for 3 b-tagged jets, at least an additional light jet and one isolated lepton) for two signal benchmark points and four dominant backgrounds, in Fig. 1. The mass-independent cutflow tables for the six benchmark points and six backgrounds are listed in Tables 2 and 3 respectively. To optimise each signal region, we impose an additional cut, viz., $0.8\,m_S < m_S^{\Delta R} < m_S+10$ GeV. In Table 4, we list the final efficiencies for each signal region after this additional cut on top of the aforementioned ones.

Finally, we show our results in Fig. 2. The left plot shows the 95 % upper limit on $BR(t \to Sc, S \to b\bar{b})$ and the right plot shows the minimum integrated luminosity to test the aforementioned branching ratio to 10^{-4} at 95 % CL.

---

[2] We did not find any significant differences when comparing with another setup using MG5_aMC@NLO v2.1.1 with the showering done with Pythia 6.
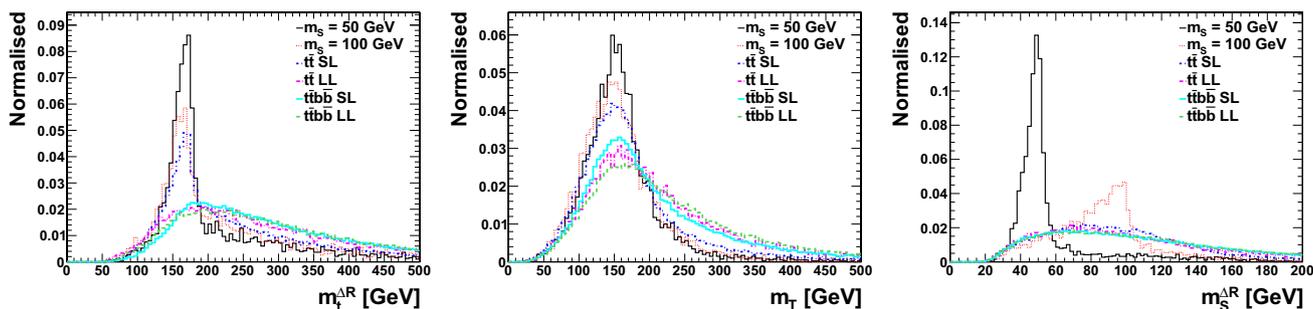
Fig. 1 (Left) The reconstructed top mass from the closest b-pair. (Center) The transverse mass m_T. (Right) The reconstructed mass of the scalar S

Table 2 Efficiency after each cut for the six signal benchmark points

Cuts	20 GeV	50 GeV	80 GeV	100 GeV	120 GeV	150 GeV
Basic	0.014	0.050	0.051	0.056	0.063	0.063
$\|\eta_{(b,\ell,j)}\| < 2.5$	0.83	0.88	0.86	0.87	0.86	0.82
ΔR(all pairs) > 0.4	0.96	0.94	0.93	0.93	0.94	0.94
$\|m_t^{\Delta R} - m_t\| < 50$ GeV	0.29	0.63	0.57	0.55	0.49	0.41
$m_T < 200$ GeV	0.72	0.56	0.87	0.85	0.83	0.74

Table 3 Efficiency after each cut for the six dominant backgrounds. SL (LL) denotes semi (di)-leptonic decays

Cuts	$t\bar{t}$ (SL)	$t\bar{t}$ (LL)	$Wb\bar{b}$	$Zb\bar{b}$	$t\bar{t}bb$ (SL)	$t\bar{t}bb$ (LL)
Basic	0.0038	0.0016	0.00032	0.00016	0.11	0.073
$\|\eta_{(b,\ell,j)}\| < 2.5$	0.78	0.69	0.74	0.71	0.90	0.85
ΔR(all pairs) > 0.4	0.95	0.94	0.95	0.95	0.96	0.91
$\|m_t^{\Delta R} - m_t\| < 50$ GeV	0.49	0.32	0.27	0.33	0.31	0.28
$m_T < 200$ GeV	0.80	0.58	0.56	0.70	0.63	0.53

Table 4 Efficiencies ($\times 10^4$) after the final cut, $0.8\, m_S < m_S^{\Delta R} < m_S + 10$ GeV, for each signal benchmark point and for the corresponding backgrounds. SL (LL) denotes semi (di)-leptonic decays

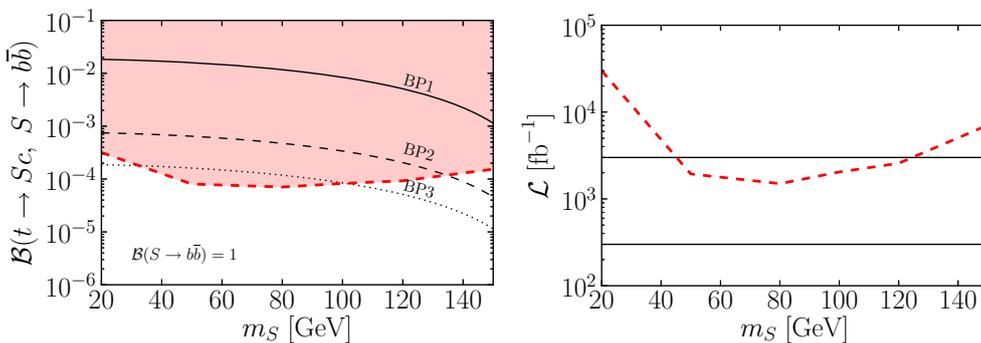| m_S (GeV)	Signal	$t\bar{t}$ (SL)	$t\bar{t}$ (LL)	$Wb\bar{b}$	$Zb\bar{b}$	$t\bar{t}bb$ (SL)	$t\bar{t}bb$ (LL)
20	8.2	0.12	0.037	0.017	0.0094	4.0	1.5
50	110	1.8	0.35	0.093	0.056	37	17
80	140	3.4	0.60	0.080	0.070	51	24
100	120	3.7	0.59	0.066	0.062	49	24
120	96	3.1	0.47	0.052	0.042	41	19
150	51	1.4	0.23	0.025	0.019	22	11

Fig. 2 (Left) Branching ratios that can be tested in the $b\bar{b}$ channel. Superimposed are the theoretical expectations in the three BPs. (Right) Luminosity required to test $\mathcal{B}(t \to Sc, S \to b\bar{b}) = 10^{-4}$. Superimposed are $\mathcal{L} = 300$ fb^{-1} and 3000 fb^{-1}
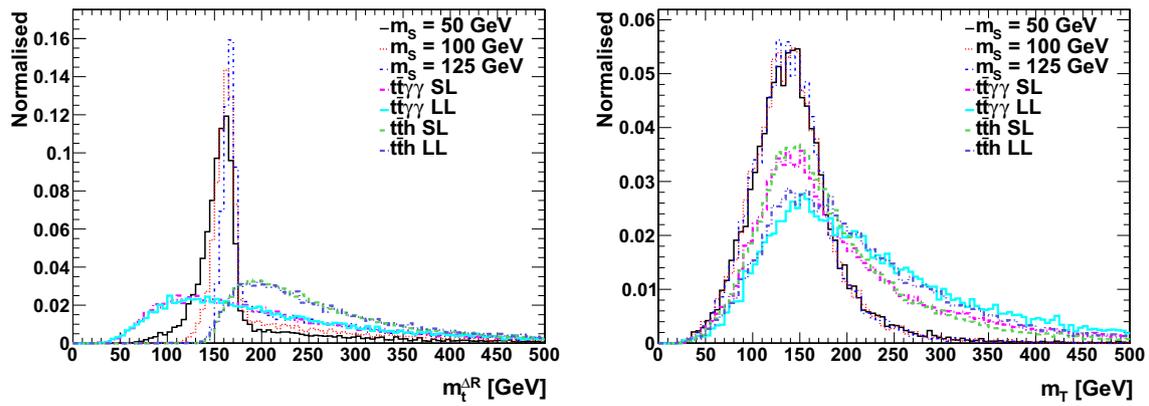
Fig. 3 (Left) The reconstructed top mass from the hardest two photons and the hardest jet. (Right) The transverse mass m_T

Table 5 Efficiency after each cut for the seven signal benchmark points

Cuts	20 GeV	50 GeV	80 GeV	100 GeV	120 GeV	125 GeV	150 GeV
Basic	0.18	0.18	0.18	0.17	0.16	0.15	0.12
$|\eta_{(b,\ell,j,\gamma)}| < 2.5$	0.91	0.91	0.91	0.90	0.89	0.88	0.83
ΔR(all pairs) > 0.4	0.62	0.91	0.91	0.90	0.88	0.88	0.87
$|m_t^{reco} - m_t| < 50$ GeV	0.81	0.78	0.77	0.74	0.65	0.61	0.33
$m_T < 200$ GeV	0.93	0.92	0.92	0.93	0.93	0.94	0.94

Table 6 Efficiency after each cut for the four dominant backgrounds. SL (LL) denotes semi (di)-leptonic decays

Cuts	$t\bar{t}\gamma\gamma$ (SL)	$t\bar{t}\gamma\gamma$ (LL)	$t\bar{t}h$ (SL)	$t\bar{t}h$ (LL)
Basic	0.18	0.12	0.26	0.16
$|\eta_{(b,\ell,j,\gamma)}| < 2.5$	0.94	0.92	0.94	0.89
ΔR(all pairs) > 0.4	0.86	0.72	0.88	0.79
$|m_t^{reco} - m_t| < 50$ GeV	0.37	0.36	0.38	0.37
$m_T < 200$ GeV	0.65	0.50	0.71	0.60

5 LHC prospects for $t \to Sc$, $S \to \gamma\gamma$

We closely follow the previous section in terms of the analysis framework. Here we focus on the scenario in which the scalar decays to a pair of photons, yielding the final state with at least two jets, with one being b-tagged, one isolated lepton and two isolated photons. Similar to the leptons, we require the photons to have $p_T > 10$ GeV and require them to lie within a pseudorapidity range of $|\eta| < 2.5$. We demand the photons to be isolated with the exact same criteria as for the leptons as discussed in the section above. The $\Delta R > 0.4$ cuts between pairs of all the selected objects are also used for this study. The dominant backgrounds for this channel are the semi-leptonic and di-leptonic $t\bar{t}h$ processes and the QCD-QED production of $t\bar{t}\gamma\gamma$. The cross section of the former is scaled by a K-factor of 1.68, what takes into account the NLO corrections to both the production and the h decay [58]. For the second, we use a conservative K-factor of 2. We also include the $W\gamma\gamma$ background matched up to two hard jets.

However, despite having a cross section of order $\mathcal{O}(0.1)$ pb, it becomes irrelevant after imposing all cuts. Consequently, we do not show explicit numbers for this process hereafter.

The selection level cuts up until the transverse mass are identical to the previous section. However, because of a much sharper diphoton mass resolution, we demand a very narrow window of 3 GeV around the scalar mass. The shape of the reconstructed top mass distributions as well as m_T in this case are shown in Fig. 3 after the basic cuts (which includes objects selected with the p_T requirement as mentioned above along with the selection criteria of exactly one b-tagged jet, at least one additional jet, one isolated lepton and two or more isolated photons). The cutflows are listed in Tables 5, 6 and 7. The 95% CL upper limit on the branching ratio $\mathcal{B}(t \to Sc, S \to \gamma\gamma)$ is shown in Fig. 4 along with the minimum integrated luminosity required to probe a branching ratio of 10^{-6}. In this analysis we have added a new m_S mass point of 125 GeV, where the $t\bar{t}h$ background is much larger. The dominance of this latter process is apparent in the figure.

Table 7 Efficiencies ($\times 10^4$) after the final cut, $|m_{\gamma\gamma} - m_S| < 3$ GeV, for each signal benchmark point and for the corresponding backgrounds. SL (LL) denotes semi (di)-leptonic decays

m_S (GeV)	Signal	$t\bar{t}\gamma\gamma$ (SL)	$t\bar{t}\gamma\gamma$ (LL)	$t\bar{t}h$ (SL)	$t\bar{t}h$ (LL)
20	760	13	5.5	0.15	0.20
50	1100	27	9.9	0.40	0.25
80	1000	19	6.8	0.45	0.35
100	940	13	5.0	0.20	0.25
120	740	6.4	3.5	0.25	0.35
125	660	5.0	2.6	570	240
150	280	2.3	1.1	0.00	0.00
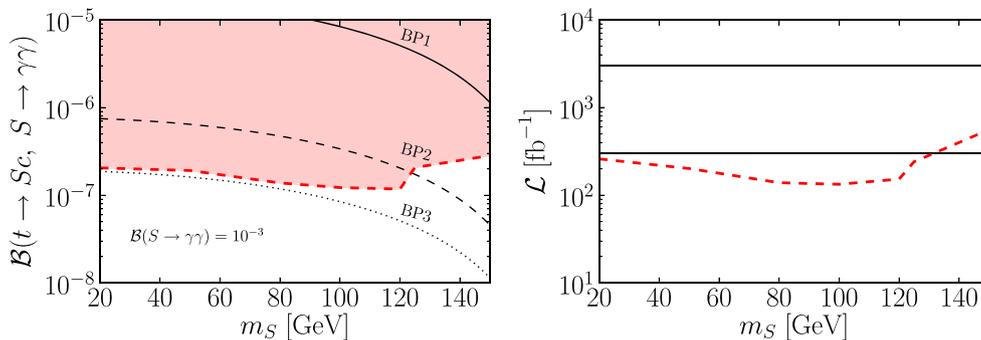
Fig. 4 (Left) Branching ratios that can be tested in the $\gamma\gamma$ channel. Superimposed are the theoretical expectations in the three BPs. (Right) Luminosity required to test $\mathcal{B}(t \to St, S \to \gamma\gamma) = 10^{-6}$. Superimposed are $\mathcal{L} = 300$ fb^{-1} and 3000 fb^{-1}

6 Conclusions

Flavour-violating top decays into scalar singlets, S, mediated by new physics at a scale $f \gtrsim \mathcal{O}(\text{TeV})$, dominate strongly over the ones involving the SM-like Higgs boson. From an effective-field theory point of view, the main reason for the dominance of the new scalar is due to the fact that the latter proceeds via effective operators of dimension six and is hence suppressed by $1/f^2$, whereas the former is already present at dimension five (and hence suppressed only by $1/f$). Moreover, the singlet can be much lighter than the Higgs, the corresponding top decay being therefore kinematically enhanced. Since such scalar particles are predicted in several new physics models, we designed novel analyses dedicated for the upcoming runs of the LHC, to search for $t \to Sc, S \to b\bar{b}/\gamma\gamma$ in events pertaining to top pair production. We restricted our study of S masses varying between 20 GeV $< m_S < 150$ GeV.

In the $S \to b\bar{b}$ channel, the highest reach is obtained for $m_S \sim 80$ GeV, for which we can probe $\mathcal{B}(t \to Sc, S \to b\bar{b}) > 10^{-4}$ at 95 % CL with an integrated luminosity of $\mathcal{L} = 3$ ab^{-1}. The reach is about a factor of 5 smaller for low masses. This is due to the fact that at low masses the two b-quarks ensuing from the scalar S, do not always form two resolved b-jets, and hence upon requiring three b-tagged jets, we incur a reduction in the efficiency of the signal. However, one might consider a fat jet in the framework of a boosted analysis to overcome this difficulty. On the other hand, for

large masses, the invariant mass of the two b-tagged jets closest in ΔR separation, do not always peak at m_S.

In the $\gamma\gamma$ channel, the sensitivity of the signal is considerably less dependent on m_S, given an excellent resolution of the di-photon mass spectrum. We find that a branching ratio, $\mathcal{B}(t \to Sc, S \to \gamma\gamma) > 10^{-7}$ can be tested at the 95 % CL with the same integrated luminosity. We note that, if $\mathcal{B}(S \to \gamma\gamma)$ is as large as $\sim 1\%$, then we can indirectly probe new physics scales as large as ~ 50 TeV. Furthermore, we note that the bound obtained in this channel for $m_S \sim m_h$ agrees well with the results obtained for $t \to hc$ listed in previous works [22] (which utilise significantly different search strategies and statistical approaches). Reference [22] also showed that the increase in sensitivity at a 100 TeV collider can be roughly estimated by scaling the signal and background cross-sections and the luminosity. In this particular channel, the dominant background is $t\bar{t}\gamma\gamma$ for masses of the singlet, m_S, well separated from m_h. It turns out that the increase in cross section in this background at $\sqrt{s} = 27$ TeV (100 TeV) with respect to that at $\sqrt{s} = 14$ TeV is similar to that in the signal, and of order $\sim 4(\sim 40)$. Thus, assuming an integrated luminosity of 10 ab^{-1}, we expect an increase in significance of order $4/\sqrt{4} \times \sqrt{10/3} \sim 3.7$ ($40/\sqrt{40} \times \sqrt{10/3} \sim 11.5$). This implies that one can expect up to an order of magnitude improvement in the bound on $\mathcal{B}(t \to Sc, S \to \gamma\gamma)$. Similar results will hold for the $b\bar{b}$ channel.

References

1. T.M.P. Tait, C.P. Yuan, Anomalous t-c-g coupling: The connection between single top production and top decay. Phys. Rev. D **55**, 7300–7301 (1997). arXiv:hep-ph/9611244
2. J. Guasch, W. Hollik, S. Penaranda, J. Sola, Single top-quark production by direct supersymmetric flavor-changing neutral-current interactions at the LHC. Nucl. Phys. Proc. Suppl. **157**, 152–156 (2006). arXiv:hep-ph/0601218
3. T. Plehn, M. Rauch, M. Spannowsky, Understanding single tops using Jets. Phys. Rev. D **80**, 114027 (2009). arXiv:0906.1803
4. M. Blanke, G.F. Giudice, P. Paradisi, G. Perez, J. Zupan, Flavoured naturalness. JHEP **06**, 022 (2013). arXiv:1302.7232
5. C. Degrande, F. Maltoni, J. Wang, C. Zhang, Automatic computations at next-to-leading order in QCD for top-quark flavor-changing neutral processes. Phys. Rev. D **91**, 034024 (2015). arXiv:1412.5594
6. R. Goldouzian, Search for top quark flavor changing neutral currents in same-sign top quark production. Phys. Rev. D **91**, 014022 (2015). arXiv:1408.0493
7. M. Backović, A. Mariotti, M. Spannowsky, Signs of tops from highly mixed stops. JHEP **06**, 122 (2015). arXiv:1504.00927
8. K. Agashe, R. Contino, Composite Higgs-mediated FCNC. Phys. Rev. D **80**, 075016 (2009). arXiv:0906.1542
9. B. Mele, S. Petrarca, A. Soddu, A new evaluation of the $t \to cH$ decay width in the standard model. Phys. Lett. B **435**, 401–406 (1998). arXiv:hep-ph/9805498
10. A. Greljo, J.F. Kamenik, J. Kopp, Disentangling flavor violation in the top-higgs sector at the LHC. JHEP **07**, 046 (2014). arXiv:1404.1278
11. A. Azatov, G. Panico, G. Perez, Y. Soreq, On the flavor structure of natural composite Higgs models & top flavor violation. JHEP **12**, 082 (2014). arXiv:1408.4525
12. CMS collaboration, V. Khachatryan et al., Search for anomalous single top quark production in association with a photon in pp collisions at $\sqrt{s}$ = 8 TeV. JHEP **04**, 035 (2016). arXiv:1511.03951
13. F.J. Botella, G.C. Branco, M. Nebot, M.N. Rebelo, Flavour changing Higgs couplings in a class of two Higgs doublet models. Eur. Phys. J. C **76**, 161 (2016). arXiv:1508.05101
14. D. Bardhan, G. Bhattacharyya, D. Ghosh, M. Patra, S. Raychaudhuri, Detailed analysis of flavor-changing decays of top quarks as a probe of new physics at the LHC. Phys. Rev. D **94**, 015026 (2016). arXiv:1601.04165
15. M. Badziak, K. Harigaya, Asymptotically free natural SUSY twin Higgs. Phys. Rev. Lett. **120**, 211803 (2018). arXiv:1711.11040
16. CMS collaboration, V. Khachatryan et al., Search for anomalous Wtb couplings and flavour-changing neutral currents in t-channel single top quark production in pp collisions at $\sqrt{s}$ = 7 and 8 TeV. JHEP **02**, 028 (2017). arXiv:1610.03545
17. E. Gabrielli, B. Mele, M. Raidal, E. Venturini, FCNC decays of standard model fermions into a dark photon. Phys. Rev. D **94**, 115013 (2016). arXiv:1607.05928
18. CMS Collaboration, Search for flavour changing neutral currents in top quark production and decays with three-lepton final state using the data collected at sqrt(s) = 13 TeV, Tech. Rep. CMS-PAS-TOP-17-017, CERN, Geneva (2017)
19. ATLAS collaboration, M. Aaboud et al., Search for flavour-changing neutral current top-quark decays $t \to qZ$ in proton-proton collisions at $\sqrt{s}$ =13 TeV with the ATLAS detector. arXiv:1803.09923
20. ATLAS collaboration, M. Aaboud et al., Search for top quark decays $t \to qH$, with $H \to \gamma\gamma$, in $\sqrt{s}$ = 13 TeV pp collisions using the ATLAS detector . JHEP **10**, 129 (2017). arXiv:1707.01404
21. ATLAS collaboration, M. Aaboud et al., Search for flavor-changing neutral currents in top quark decays $t \to Hc$ and $t \to Hu$ in multilepton final states in proton–proton collisions at $\sqrt{s}$ = 13 TeV with the ATLAS detector. arXiv:1805.03483
22. A. Papaefstathiou, G. Tetlalmatzi-Xolocotzi, Rare top quark decays at a 100 TeV protonproton collider: $t \to bWZ$ and $t \to hc$. Eur. Phys. J. C **78**, 214 (2018). arXiv:1712.06332
23. N. Craig, J.A. Evans, R. Gray, M. Park, S. Somalwar, S. Thomas, Searching for $t \to ch$ with multi-Leptons. Phys. Rev. D **86**, 075002 (2012). arXiv:1207.6794
24. R. Harnik, J. Kopp, J. Zupan, Flavor violating Higgs decays. JHEP **03**, 026 (2013). arXiv:1209.1397
25. ATLAS, CMS collaboration, G. Aad et al., Measurements of the Higgs boson production and decay rates and constraints on its couplings from a combined ATLAS and CMS analysis of the LHC pp collision data at $\sqrt{s}$ = 7 and 8 TeV . JHEP **08**, 045 (2016). arXiv:1606.02266
26. S. Banerjee, M. Mitra, M. Spannowsky, Searching for a heavy Higgs boson in a Higgs-portal B-L Model. Phys. Rev. D **92**, 055013 (2015). arXiv:1506.06415
27. DELPHI, OPAL, ALEPH, LEP Electroweak Working Group, L3 collaboration, J. Alcaraz et al., A combination of preliminary electroweak measurements and constraints on the standard model. arXiv:hep-ex/0612034
28. CDF collaboration, T. Aaltonen et al., Precise measurement of the W-boson mass with the CDF II detector. Phys. Rev. Lett. **108**, 151803 (2012). arXiv:1203.0275
29. D0 collaboration, V.M. Abazov et al., Measurement of the W boson mass with the D0 detector. Phys. Rev. D **89**, 012005 (2014). arXiv:1310.8628
30. T. Robens, T. Stefaniak, Status of the Higgs singlet extension of the standard model after LHC Run 1. Eur. Phys. J. C **75**, 104 (2015). arXiv:1501.02234
31. D. Lpez-Val, T. Robens, r and the W-boson mass in the singlet extension of the standard model. Phys. Rev. D **90**, 114018 (2014). arXiv:1406.1043
32. M.E. Peskin, Comparison of LHC and ILC capabilities for Higgs Boson coupling measurements. arXiv:1207.2516
33. N. Craig, H.K. Lou, M. McCullough, A. Thalapillil, The Higgs portal above threshold. JHEP **02**, 127 (2016). arXiv:1412.0258
34. U. Ellwanger, C. Hugonie, A.M. Teixeira, The next-to-minimal supersymmetric standard model. Phys. Rept. **496**, 1–77 (2010). arXiv:0910.1785
35. S. Dimopoulos, J. Preskill, Massless composites with massive constituents. Nucl. Phys. B **199**, 206–222 (1982)
36. D.B. Kaplan, H. Georgi, SU(2) x U(1) breaking by vacuum misalignment. Phys. Lett. B **136**, 183–186 (1984)
37. D.B. Kaplan, H. Georgi, S. Dimopoulos, Composite Higgs scalars. Phys. Lett. B **136**, 187–190 (1984)
38. G. Panico, A. Wulzer, The composite Nambu–Goldstone Higgs. Lect. Notes Phys. **913**, 1–316 (2016). arXiv:1506.01961

39. C. Zhang, F. Maltoni, Top-quark decay into Higgs boson and a light quark at next-to-leading order in QCD. Phys. Rev. D **88**, 054005 (2013). arXiv:1305.7386

40. UTfit collaboration, M. Bona et al., Model-independent constraints on $\Delta F = 2$ operators and the scale of new physics. JHEP **03**, 049 (2008). arXiv:0707.0636

41. Top Quark Working Group collaboration, K. Agashe et al., Working Group Report: Top Quark, in *Proceedings, 2013 Community Summer Study on the Future of U.S. Particle Physics: Snowmass on the Mississippi (CSS2013): Minneapolis, MN, USA, July 29–August 6, 2013* (2013). arXiv:1311.2028

42. CMS collaboration, Search for the flavor-changing interactions of the top quark with the Higgs boson in $H \rightarrow b\bar{b}$ channel at $\sqrt{s} = $ 13 TeV, CMS-PAS-TOP-17-003 (2017)

43. Particle Data Group collaboration, C. Patrignani et al., Review of particle physics. Chin. Phys. C **40**, 100001 (2016)

44. B. Gripaios, A. Pomarol, F. Riva, J. Serra, Beyond the minimal composite Higgs model. JHEP **04**, 070 (2009). arXiv:0902.1483

45. G. Ferretti, D. Karateev, Fermionic UV completions of composite Higgs models. JHEP **03**, 077 (2014). arXiv:1312.5330

46. M. Chala, R. Grber, M. Spannowsky, Searches for vector-like quarks at future colliders and implications for composite Higgs models with dark matter. JHEP **03**, 040 (2018). arXiv:1801.06537

47. G.C. Branco, D. Emmanuel-Costa, R. Gonzalez, Yukawa structure with maximal predictability. Phys. Lett. B **483**, 87–93 (2000). arXiv:hep-ph/9905290

48. R.G. Roberts, A. Romanino, G.G. Ross, L. Velasco-Sevilla, Precision test of a fermion mass texture. Nucl. Phys. B **615**, 358–384 (2001). arXiv:hep-ph/0104088

49. CMS collaboration, V. Khachatryan et al., Search for Higgs boson off-shell production in proton-proton collisions at 7 and 8 TeV and derivation of constraints on its total decay width. JHEP **09**, 051 (2016). arXiv:1605.02329

50. J.E. Kim, H.P. Nilles, The mu problem and the strong CP problem. Phys. Lett. B **138**, 150–154 (1984)

51. J. Alwall, R. Frederix, S. Frixione, V. Hirschi, F. Maltoni, O. Mattelaer, The automated computation of tree-level and next-to-leading order differential cross sections, and their matching to parton shower simulations. JHEP **07**, 079 (2014). arXiv:1405.0301

52. M.L. Mangano, M. Moretti, F. Piccinini, M. Treccani, Matching matrix elements and shower evolution for top-quark production in hadronic collisions. JHEP **01**, 013 (2007). arXiv:hep-ph/0611129

53. LHC Physics: NNLO+NNLL top-quark-pair cross sections. https://twiki.cern.ch/twiki/bin/view/LHCPhysics/TtbarNNLO Accessed 22 Aug 2018

54. R.D. Ball, Parton distributions with LHC data. Nucl. Phys. B **867**, 244–289 (2013). arXiv:1207.1303

55. T. Sjöstrand, S. Ask, J.R. Christiansen, R. Corke, N. Desai, P. Ilten, An Introduction to PYTHIA 8.2. Comput. Phys. Commun. **191**, 159–177 (2015). arXiv:1410.3012

56. M. Cacciari, G.P. Salam, G. Soyez, The Anti-k(t) jet clustering algorithm. JHEP **04**, 063 (2008). arXiv:0802.1189

57. M. Cacciari, G.P. Salam, G. Soyez, FastJet user manual. Eur. Phys. J. C **72**, 1896 (2012). arXiv:1111.6097

58. LHCPhysics (2014). http://twiki.cern.ch/twiki/bin/view/lhcphysics/cernyellowreportpageat1314tev2014